C. R. Physique 14 (2013) 306–317

Contents lists available at SciVerse ScienceDirect

Comptes Rendus Physique

www.sciencedirect.com

Gravitational waves / Ondes gravitationnelles

Numerical simulations of black-hole binaries and gravitational wave emission

Ulrich Sperhake [a,b,c,d,e,*], Emanuele Berti [b,d], Vitor Cardoso [c,d]

[a] Institute of Space Sciences (CSIC–IEEC), Campus UAB, Torre C5 parells, 08193 Bellaterra, Spain
[b] California Institute of Technology, 1200 E California Boulevard, Pasadena, CA 91125, USA
[c] CENTRA, Departamento de Física, Instituto Superior Técnico, Universidade Técnica de Lisboa – UTL, Av. Rovisco Pais 1, 1049 Lisboa, Portugal
[d] Department of Physics and Astronomy, The University of Mississippi, University, MS 38677, USA
[e] Department of Applied Mathematics and Theoretical Physics, University of Cambridge, Cambridge CB3 0WA, UK

ARTICLE INFO

Article history:
Available online 16 February 2013

Keywords:
Numerical relativity
Black holes
Gravitational wave physics
Astrophysics

Mots-clés :
Relativité numérique
Trous noirs
Physique des ondes gravitationnelles
Astrophysique

ABSTRACT

We review recent progress in numerical relativity simulations of black-hole (BH) spacetimes. Following a brief summary of the methods employed in the modeling, we summarize the key results in two major areas of BH physics: (i) BHs as sources of gravitational waves (GWs) and (ii) astrophysical systems involving BHs. We conclude with a list of the most urgent tasks for numerical relativity in these areas.

© 2013 Académie des sciences. Published by Elsevier Masson SAS. All rights reserved.

RÉSUMÉ

Nous passons en revue les progrès récents concernant la simulation des trous noirs en relativité numérique. Après un bref résumé des méthodes employées, nous donnons les résultats clés dans deux domaines majeurs de la physique des trous noirs : (i) les trous noirs comme sources d'ondes gravitationnelles et (ii) les systèmes astrophysiques contenant des trous noirs. Nous concluons sur la liste des travaux les plus urgents à conduire dans ces domaines.

© 2013 Académie des sciences. Published by Elsevier Masson SAS. All rights reserved.

1. Introduction

For almost a century now after its discovery, the Schwarzschild solution describing a static, spherically symmetric vacuum spacetime in Einstein's theory of general relativity (GR) has been a valuable tool for a wealth of theoretical and experimental studies. For more than half a century, the validity of the solution beyond the Schwarzschild radius $r = 2GM/c^2$ and the consequent existence of BHs was thought to be a mathematical artifact of the field equations. This picture has changed dramatically in more recent decades. Crucial events in this sense were the astrophysical X-ray and radio observations in the 1960s and 1970s. Cosmic X-ray sources, first detected in 1963 [1], were soon associated with compact stellar objects and, in particular, with mass exchange from an ordinary star onto a compact object in binary systems [2]. Over the following years, the explanation of these systems in terms of accretion onto compact stellar objects in binary systems became widely accepted (see [3] for a review).

Also starting in the early 1960s, optical and radio observations identified "star-like" objects with surprisingly large redshifts [4,5]. If interpreted as cosmological in origin, the redshifts implied enormous distances and, accordingly, luminosities.

* Corresponding author at: Department of Applied Mathematics and Theoretical Physics, University of Cambridge, Cambridge CB3 0WA, UK.
E-mail address: sperhake@tapir.caltech.edu (U. Sperhake).

1631-0705/$ – see front matter © 2013 Académie des sciences. Published by Elsevier Masson SAS. All rights reserved.
http://dx.doi.org/10.1016/j.crhy.2013.01.004

Over the ensuing decade the cosmological origin of these "quasi-stellar" sources (or quasars) became clear, and accretion onto supermassive BHs (SMBHs) [6,7] was accepted as the most plausible explanation of their energetics [8,9].

Electromagnetic observations provide strong but *indirect* evidence for the existence of astrophysical BHs. A more direct way of probing the BH nature of astrophysical compact objects is offered by the newly emerging field of GW astronomy. First-generation ground-based laser-interferometric detectors (such as LIGO, VIRGO and GEO600) have reached design sensitivity, and advanced versions of these detectors will be operational within a few years [10–12]. One of the most prominent sources of detectable GWs for these detectors is the inspiral and coalescence of stellar-mass and intermediate-mass BH (IMBH) binaries. At lower frequencies, space-based laser-interferometric observations [13] have the potential to complement ground-based efforts with high signal-to-noise ratio observations of massive BH binaries. Due to the weak interaction of GWs with any type of matter, including the detectors, digging physical signals from the noisy data stream represents a daunting task and heavily relies on so-called *matched filtering* techniques [14]. Matched filtering is a common choice to search for signals of known form in noisy data, and works by cross-correlating the actual "signal" (i.e., the detector's output) with a set of theoretical templates. Accurate modeling of the GW sources thus plays a vital role in maximizing the scientific output from these experimental efforts.

Event rate estimates for IMBHs and stellar-mass BH binaries are very uncertain, but advanced Earth-based detectors are expected to observe several events per year (see [15] for a review). The observations of two possible X-ray binary precursors of BH–BH binaries provide a much needed observational constraint on compact binaries containing at least one BH, suggesting again that BH–BH binary mergers may be more common than anticipated [16]. Estimates for event rates of SMBH binaries detectable by space-based interferometers range from 0.1 to 1000s per year, with a most likely estimate of ~ 20–30 [17–20].

For many of these scenarios, it is convenient to divide the coalescence of a BH binary in the framework of GR into three stages which mirror the different tools used for their modeling: (i) The inspiral phase, where the interaction between the individual holes is still sufficiently weak to justify the use of post-Newtonian (PN) techniques [21]; (ii) The final orbits, plunge and merger, which are governed by the strong-field regime of Einstein's equations and can be described only by fully numerical simulations; (iii) The ringdown of the remnant BH, which is amenable to a perturbative treatment [22–24].

In this article we will focus on the second, strong-field stage, the numerical tools dedicated to its study, and results obtained following the 2005 breakthroughs [25–27]. As we shall see, however, a comprehensive understanding of BH dynamics requires a close interplay of numerical and analytical studies, and we will discuss in various cases the interface between numerical relativity and approximation techniques.

Following a brief summary of the framework employed in numerical relativity (Section 2), in Sections 3 and 4 we will present the main results obtained from numerical studies of BHs in the context of GW detection and astrophysics, respectively. We conclude in Section 5 with a discussion of future applications of numerical relativity.

Notation We shall be using geometrical units, such that the gravitational constant $G = 1$ and the speed of light $c = 1$. We denote spacetime indices $0 \ldots 3$ by Greek letters, and spatial indices $1 \ldots 3$ by Latin letters.

2. Numerical modeling of black holes

In Einstein's GR, spacetime is modeled as a four-dimensional manifold with a metric $g_{\alpha\beta}$ of Lorentzian signature $-+++$, corresponding to three spatial and one time dimension. The metric is determined by the Einstein equations

$$G_{\alpha\beta} \equiv R_{\alpha\beta} - \frac{1}{2} g_{\alpha\beta} R = T_{\alpha\beta} \tag{1}$$

with $T_{\alpha\beta} = 0$ in vacuum. While analytic solutions (as, for example, the Schwarzschild and Kerr solutions and the Friedmann–Lemaître–Robertson–Walker solution) have been found for systems with high symmetry, solutions for dynamical configurations without special symmetries generally require the use of numerical tools. For this purpose the Einstein equations need to be cast as an *initial value formulation*. In the following we will discuss two approaches which provide an initial value formulation of the Einstein equations and have led to successful, long-term stable numerical evolutions: the generalized harmonic (GH) formulation employed in Pretorius' breakthrough BH binary simulations [25] and the canonical Arnowitt–Deser–Misner (ADM) split [28], reformulated by York [29], which forms the starting point for the *moving puncture* breakthroughs [26,27].

2.1. 3+1 split

Spacetime is decomposed into a one-parameter family of three-dimensional spatial slices. We choose coordinates adapted to this formulation, such that the coordinate time t labels each slice and x^i denotes points on the slice. On each hypersurface, there exists a unique timelike, future pointing unit normal field n^α which defines a projection operator $\perp^\alpha{}_\beta = g^\alpha{}_\beta + n^\alpha n_\beta$ onto the hypersurface. The geometry of the hypersurface is completely determined by the *three-metric* or *first fundamental form* $\gamma_{ij} \equiv \perp^\mu{}_i \perp^\nu{}_j g_{\mu\nu} = g_{ij}$. The coordinate freedom is represented by the shift vector $\beta_i \equiv g_{ti}$ and the lapse function $\alpha \equiv \sqrt{g_{tt} - \beta^m \beta_m}$ (with $\beta^i \equiv \gamma^{im} \beta_m$), which relate spatial coordinates on (and measure separation in proper time between)

different hypersurfaces. The projections $\perp^{\alpha}{}_{i}\perp^{\beta}{}_{j}G_{\alpha\beta}$, $\perp^{\alpha}{}_{i}G_{\alpha\mu}n^{\mu}$, $G_{\mu\nu}n^{\mu}n^{\nu}$ of the Einstein equations then lead to six evolution equations for the three-metric γ_{ij}, three momentum constraints and the Hamiltonian constraint:

$$\partial_t \gamma_{ij} = \beta^m \partial_m \gamma_{ij} + \gamma_{mi}\partial_j \beta^m + \gamma_{mj}\partial_i \beta^m - 2\alpha K \tag{2}$$

$$\partial_t K_{ij} = \beta^m \partial_m K_{ij} + K_{mi}\partial_j \beta^m + K_{mj}\partial_i \beta^m - D_i D_j \alpha + \alpha\big(\mathcal{R}_{ij} + K K_{ij} - 2K_{im}K^m{}_j\big) \tag{3}$$

$$\mathcal{H} \equiv \mathcal{R} + K^2 - K_{mn}K^{kn} = 0 \tag{4}$$

$$\mathcal{M}^i \equiv D_m\big(K^{im} - \gamma^{im}K\big) = 0 \tag{5}$$

where $\mathcal{R}_{ij}$, $\mathcal{R}$ and D_i denote the Ricci tensor, Ricci scalar and covariant derivative associated with the three-metric, and the extrinsic curvature K_{ij} has been introduced to obtain a first-order system in time.

It turns out that this formulation of the Einstein equations is only *weakly hyperbolic* [30], and therefore not suitable for long-term stable numerical evolutions. Motivated by these stability problems, several modifications of the ADM system have been investigated. The most popular is the Baumgarte–Shapiro–Shibata–Nakamura (BSSN) formulation [31,32], which rearranges the degrees of freedom via a split of the extrinsic curvature into trace and trace-free parts, a conformal transformation and promotion of the contracted conformal Christoffel symbols to the status of independent variables:

$$\begin{aligned}
&\phi = \frac{1}{12}\ln\gamma, \qquad \tilde{\gamma}_{ij} = e^{-4\phi}\gamma_{ij} \\
&K = \gamma^{ij}K_{ij}, \qquad \tilde{A}_{ij} = e^{-4\phi}\left(K_{ij} - \frac{1}{3}\gamma_{ij}K\right) \\
&\tilde{\Gamma}^i = \tilde{\gamma}^{mn}\tilde{\Gamma}^i_{mn} = \frac{1}{2}\tilde{\gamma}^{mn}\tilde{\gamma}^{ik}(\partial_m\tilde{\gamma}_{nk} + \partial_n\tilde{\gamma}_{km} - \partial_k\tilde{\gamma}_{mn})
\end{aligned} \tag{6}$$

The resulting set of evolution and constraint equations is given in Eqs. (15)–(30) of [33], and is employed in the present generation of moving puncture evolution codes which fix the gauge via "1 + log" slicing and the Γ-driver condition [33–36].

2.2. GH formulation

Harmonic coordinates are defined by the condition $g_{\alpha\mu}\Box x^{\mu} = -\Gamma_{\alpha} = 0$, where $\Box \equiv \nabla^{\mu}\nabla_{\mu}$ represents the scalar wave operator. These coordinates have played an important role in the analysis of the Cauchy problem in GR [37–39]. In harmonic coordinates, the Einstein equations take on a manifestly hyperbolic form, which allows for a generalization to arbitrary coordinate or gauge choices [40,41]. The first step is to introduce four arbitrary source functions H^{α} such that the coordinates obey

$$-\Gamma^{\alpha} = \Box x^{\alpha} = H^{\alpha} \tag{7}$$

and treat these functions as independent evolution variables. Then one considers the GH system:

$$R_{\alpha\beta} - \nabla_{(\alpha}C_{\beta)} = 0 \tag{8}$$

where $C_{\alpha} \equiv H_{\alpha} + \Gamma_{\alpha}$. Eq. (8) is equivalent to the Einstein equations, subject to the validity of the constraints (7) which are preserved by virtue of the Bianchi identities provided that C_{α} and $\partial_t C_{\alpha}$ vanish on the initial hypersurface $t = 0$. A key ingredient in the numerical evolution of the GH system is the addition of a constraint damping term to the evolution equations [42].

The spectral code originally developed by the Caltech–Cornell group (see [43,44] and references therein) employs a first-order version of the GH system [45] with dual-coordinate frames and BH excision. While more complex in structure, this framework enables their code to generate BH evolutions with exceptional accuracy [46,47].

2.3. Initial data

The construction of initial data requires solving the Hamiltonian and momentum constraints. Here we only summarize the key concepts; we refer the reader to Cook's review article [48] for details. Most work on the construction of initial data is based on the York–Lichnerowicz split [29,49], which involves a conformal transformation of metric and extrinsic curvature and separates the latter into trace and trace-free part. The resulting elliptic equations simplify substantially under the assumption of conformal flatness and a spatially constant K.

While this formalism provides a convenient method to solve the constraint equations, we still need to ensure that the initial data represent a physically realistic system, typically two BHs with specific spins and momenta. This can be achieved by generalizing the Schwarzschild solution, which is obtained in the above framework in conformally flat form with conformal factor $\exp(\phi) = 1 + \frac{m}{2r}$. A generalization to initial data of N BHs starting from rest is directly obtained by the construction of Misner [50] or Brill and Lindquist [51]. Remarkably, an analytic solution for the extrinsic curvature can still be obtained for BHs with initial linear momenta $\mathbf{P}_n$ and spins $\mathbf{S}_n$ [52]. By applying a compactification to the

internal asymptotically flat region, Brandt and Brügmann [53] arrived at the so-called *puncture data* construction, which is the method of choice for most numerical evolutions employing the BSSN formulation.

In alternative to generalizing analytically known BH solutions, the presence of horizons in the initial data can be encoded in the form of boundary conditions for the metric and extrinsic curvature [54,55] as determined by the isolated horizon framework [56]. Initial data along these lines have been constructed in [54,55], and form the starting point of most of the numerical evolutions using the GH system (see e.g. [44,57]).

2.4. Diagnostics

Extracting physical information from numerical simulations of the Einstein equations is nontrivial for two reasons. First, the evolved variables are dependent on the coordinate conditions; second, it is often not possible to define local quantities familiar from Newtonian physics. The first difficulty requires the calculation of gauge-independent variables. The second difficulty is alleviated by the *isolated horizon* framework [56], which facilitates the calculation of BH mass and spin in the limit of isolated BHs.

In comparison, it is more straightforward to extract global quantities of the spacetime, most notably the total mass–energy $M_{\rm ADM}$ and the linear and angular momentum P_i, J_i [28,29]. These are given by surface integrals at spatial infinity, see e.g. Eqs. (7.15), (7.56) and (7.63) in [58].

Local properties of the BHs are encoded in their apparent horizon [59–62]. In particular, the irreducible mass can be expressed in terms of the apparent horizon area: $M_{\rm irr} = \sqrt{A_{\rm AH}/16\pi}$. In the limit of an isolated BH, the spin can be derived from the integration of the rotational Killing vectors over the horizon according to Eq. (8) of [62].

Arguably the most important diagnostic quantity in BH simulations is the GW signal. The most common method to extract GWs is based on the Newman–Penrose formalism [63] and derives the complex Newman–Penrose scalar Ψ_4 from contraction of the Weyl tensor with suitably chosen tetrad vectors [64], Section III A in [65]. It is often convenient to decompose Ψ_4 into multipoles ψ_{lm} using spherical harmonics of spin-weight -2: $\Psi_4(t,r,\theta,\phi) = \sum_{l=2}^{\infty} {}_{-2}Y_{lm}(\theta,\phi)\psi_{lm}(t,r)$. From Ψ_4, one straightforwardly obtains the energy, linear and angular momentum radiated in the form of GWs; see e.g. Eqs. (49)–(51) in [65]. In GW data analysis it is more common to work with the wave strain

$$h \equiv h_+ - ih_\times = \int_{-\infty}^{t} \mathrm{d}t' \int_{-\infty}^{t'} \mathrm{d}t'' \Psi_4 \tag{9}$$

decomposed into multipoles: $h(t,r,\theta,\phi) = \sum_{l=2}^{\infty} {}_{-2}Y_{lm}(\theta,\phi) h_{lm}(t,r)$.

Alternatively, GWs can be extracted by viewing the metric in the far field regime as a perturbation of the Schwarzschild spacetime and employing the formalism of Regge, Wheeler [66] and Zerilli [67,68]. One thus obtains the Regge–Wheeler–Moncrief and Zerilli–Moncrief master functions $Q^{\times}_{lm}$, Q^{+}_{lm}, which can be converted into the multipolar components of the GW strain h according to Eq. (49) of [69].

3. Gravitational wave physics

BH binary systems represent one of the most promising sources of detectable GWs. The parameters of a BH binary are commonly divided into *intrinsic* and *extrinsic* [70]. Intrinsic parameters characterize physical properties of the system, such as the total mass M, the mass ratio $q \equiv M_2/M_1 \leqslant 1$, the individual BH spins $\mathbf{S}_1$, $\mathbf{S}_2$ and the orbital eccentricity. Extrinsic parameters such as sky position, distance, orbital inclination angle, arrival time and initial phase of the wave, in contrast, depend on the source location relative to the observer, and do not directly enter the GW source modeling process.

The majority of numerical studies of BH binary spacetimes performed to date have focussed on comparable mass ratios $q \lesssim 1/10$ and moderate spin magnitudes $\chi_i \equiv |\mathbf{S}_i|/M_i^2 \lesssim 0.8$, with particular emphasis on spins (anti-)aligned with the orbital angular momentum. We note, however, the following explorations outside this "best charted" subset of the parameter space. Circular binaries with mass ratios up to $q = 1/100$ have been studied in [71,72]. BH binaries with spins ~ 0.9 have been evolved in [73–75], but exceeding an apparent barrier of $\chi \approx 0.93$ requires departure from the conformal flatness assumption [76–78]. Finally, we note that emission of GWs efficiently circularizes BH binary orbits [79]. BH binaries are therefore expected to have vanishing eccentricity by the time they enter the frequency window of ground-based detectors, and for this reason most work on GW source modeling has focussed on the quasi-circular limit.

3.1. Gravitational waveforms from BH binaries

For illustration, we display in Fig. 1 the real parts of the h_{22} and h_{33} multipoles of the GW strain h obtained for the inspiral and coalescence of a binary of nonspinning BHs with mass ratio $q = 1/4$ [80]. In the course of the inspiral, both amplitude and frequency of the GW signal gradually increase. Close to merger, defined as formation of a common apparent horizon, the GW amplitude reaches a maximum. Eventually it drops exponentially as the merged hole rings down to a stationary Kerr state: see e.g. Fig. 18 in [57].

The qualitative features of the GW signal emitted by different types of binaries can be summarized as follows. (i) The inspiral of two nonspinning, equal-mass BHs is the case most intensively studied by numerical relativity. The wave signal

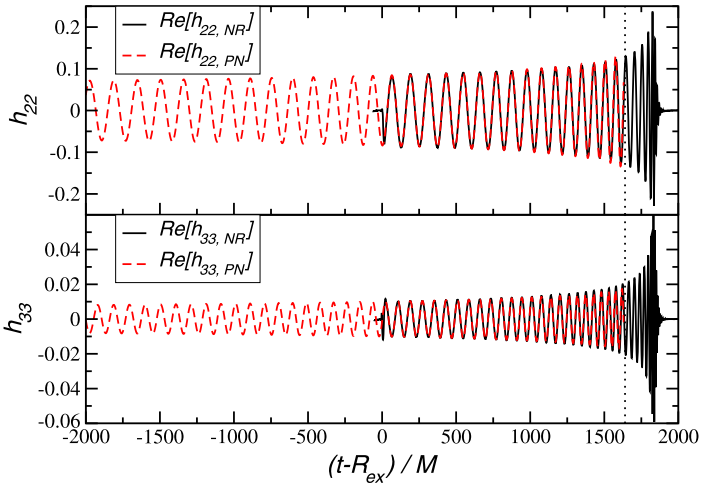

Fig. 1. Real part of the GW multipoles h_{22} and h_{33} obtained from the inspiral and merger of a nonspinning binary with mass ratio $q = 1/4$. The dashed red curve represents PN predictions matched to the numerical (solid black) signal. The vertical dotted lines mark the time when the frequency of the $(l, m) = (2, 2)$ multipole has reached $M\omega = 0.1$. (Please refer to the online version for interpretation of color indications.)

is dominated by the $(l, m) = (2, 2)$ multipolar component, which carries $> 98\%$ of the total radiated energy. The longest numerical simulation by Scheel et al. [81] covers 16 orbits and reports a ratio of final to initial BH mass $M_f/M = 0.95162 \pm 0.00002$ and a final spin $S_f/M_f^2 = 0.68646 \pm 0.00004$. (ii) As the mass ratio decreases, higher-order modes become more prominent [82] and the fractional energy in $(l, m) = (2, 2)$ drops to about 68% in the limit $q \to 0$ [83]. Motivated by the strong relation of phase and frequency of different (l, m) multipoles, Baker et al. [84] view the (l, m) radiation modes as being generated by the corresponding momenta of an *implicit rotating source*. (iii) GW multipoles with odd l are suppressed in the equal-mass limit due to symmetry. (iv) BH binaries with spins aligned with the orbital angular momentum emit stronger GW signals due to an effect sometimes referred to as *orbital hang-up*: equal-mass binaries with $\chi_1 = \chi_2 = 0.757$ radiate about twice as much energy and angular momentum when compared to the nonspinning case [85]. For anti-aligned spins the GW energy decreases by a similar factor. (v) Orbital eccentricity introduces a nonmonotonic behavior of the GW frequency; cf. Fig. 6 in [86]. (vi) Spin–spin and spin–orbit couplings cause a precession of the orbital plane in the case of BH binaries with spins that are not aligned or anti-aligned with the orbital angular momentum. This precession manifests itself in a modulation of the GW amplitude emitted in a fixed angular direction: cf. Fig. 1 in [87].

3.2. Tests of general relativity

Numerical simulations of binary BH mergers provide an opportunity to study the nonlinearities of the theory and to test the Kerr nature of astrophysical BHs. If GR is the correct theory of gravitation, all BHs in the Universe should be described by the Kerr solution [88], which depends on two parameters: the mass M and the dimensionless spin χ. The remnant of a binary BH merger settles down to the Kerr solution by emitting gravitational radiation at characteristic (complex) quasinormal frequencies $M\omega_{nlm}$ that depend only on χ. Here (l, m) are the usual angular indices, and n is the "overtone number": modes with small n have a longer damping time and should dominate the radiation [24,89].

The measurement of the real and imaginary part of a single quasinormal mode contains, in principle, enough information to determine the mass and spin of the BH. Together with the accurate determination of the individual BH masses from the inspiral phase this already allows for tests of GR, by testing the GR prediction for mass loss during inspiral and merger and at the same time the strong-field dynamics of GR. The measurement of *any* other frequency or damping time then provides a further interesting test of the Kerr nature of the final BH [90]. The feasibility of these tests depends on the characteristics of a given GW detector and on the relative excitation of the modes (see [91,92] for detailed studies). Quantifying the excitation of quasinormal modes for generic initial data is a formidable technical problem [23,93], but numerical merger simulations allow sensible estimates of the relative quasinormal mode amplitudes [57,82]. The relative mode amplitude depends on the binary parameters, and therefore, in principle, the measurement of a multi-mode signal with single or (better) multiple GW detectors can be used to measure the binary mass ratio or the inclination of the final BH spin with respect to the line of sight.

We also remark that the increased signal-to-noise ratio coming from the merger has been shown to *improve* the bounds on alternative theories of gravity that could come from observations of the inspiral only. Keppel and Ajith, for example, discussed this possibility in the context of massive graviton theories, where the graviton mass would modify the dispersion relation of GWs [94]. Formulations of the evolution equations in alternative theories of gravity are in their infancy [95,96]. This is an interesting line of research, and in the near future we may have more concrete ways to quantify deviations from GR in strong-field mergers.

3.3. GW template banks

The key challenge in GW data analysis is to accurately predict and isolate the features of gravitational waveforms in the data stream from GW detectors. This is necessary in order to (i) detect the presence of a GW signal of astrophysical origin, and (ii) determine the parameters of the emitting source. These goals can be achieved by matched filtering, i.e. by cross-correlating the data stream s (composed of detector noise n plus a potential GW signal h) with a bank of theoretical waveform templates h_{λ_i}, where the indices λ_i $(i = 1, \ldots, P)$ denote the P intrinsic and extrinsic source parameters. For this purpose it is imperative to construct a large set of accurate numerical waveforms which cover the relevant parameter space. This task far exceeds the capacity of purely numerical methods. Because current numerical simulations cover only about 30 cycles of the inspiral, the generation of complete waveforms requires the combined use of PN and numerical methods. The construction of such GW template banks currently proceeds along either of the following two paths.

(i) The *effective-one-body* (EOB) approach [97,98] maps the dynamics of the two-body problem in GR into the motion of a particle in an effective metric. The components of the effective metric are currently determined to 3PN order. The EOB method improves upon this model by using additional *pseudo-PN* terms of higher order which are not derived from PN expressions, but calibrated via comparison with numerical results [99–103]. The inspiral–plunge waveform resulting from this construction is then matched to a merger–ringdown signal composed of a superposition of quasinormal oscillation modes of a Kerr BH. The total number of free parameters varies between the individual EOB models currently investigated, but in all cases, the general strategy is to calibrate these parameters by comparison with a finite number of numerical simulations.

(ii) *Phenomenological waveform templates* are based on *hybrid waveforms*: the early inspiral is modeled by PN techniques, and the resulting signal is matched (within a specified window) to a numerical waveform describing the last orbits, merger and ringdown. The resulting set of hybrid waveforms are then approximated by a model containing a number of phenomenological parameters which are mapped to the physical parameters of the binaries. The phenomenological models initially developed for nonspinning binaries in [104–106], and then extended to the case of spins aligned with the orbital angular momentum [107], are based on hybrid waveforms matched in the *time domain*, whereas the more recent study by Santamaria et al. [108] performs the matching in the frequency domain. In spite of such differences in their construction, the final result of all these phenomenological models are closed-form analytic expressions for the waveforms in the frequency domain.

Both types of template banks are employed in the analysis of GW data. The recent search for GWs from binary BH inspiral, merger and ringdown [109] used phenomenological models for injection, and an EOB model for injection and for the search templates. Numerical waveforms have also been used inside the GW community-wide *Ninja* project [110] to study the sensitivity of existing GW search algorithms used in the analysis of observational data [111,112]. A further community-wide effort, the *NRAR* project [113], is dedicated to a systematic exploration of the complete BH binary parameter space to develop optimally-calibrated template families to be used in GW data analysis.

One of the most exciting prospects of GW detection is the idea of looking for electromagnetic counterparts to the GW signal. The inclusion of merger and/or of higher multipolar components of the radiation in the waveform models has been shown to provide significant improvements in source localization and distance determination [114,115]. For this reason it is very important to construct phenomenological models including higher multipoles of the full inspiral/merger/ringdown waveform. The EOB model has recently been extended in this direction [99].

3.4. Accuracy requirements

Clearly, the two approaches for template construction mentioned above require accurate numerical waveforms. Quantifying these accuracy requirements is a nontrivial task. Numerical uncertainties due to finite resolution are directly tested by *convergence analysis*, and the error incurred by extracting GWs at finite radius can be estimated using extrapolation of results from various radii to infinity [116]. It is most convenient to measure accuracy and agreement of different waveforms in terms of quantities which automatically take into account the relative alignment in time and phase between waveforms. Such a measure is obtained from the inner product between two waveforms $h(t)$ and $g(t)$ used in the theory of parameter estimation [117,118]:

$$\langle h, g\rangle \equiv 4\mathbf{Re}\int_0^\infty \frac{\tilde{h}(f)\tilde{g}^*(f)}{S_{\mathrm{N}}(f)}\,\mathrm{d}f \tag{10}$$

where the tilde and asterisk denote the Fourier transform and complex conjugate, respectively, and $S_{\mathrm{N}}(f)$ is the one-sided power spectral density of the detector strain noise [119]. In practice, this inner product is to be understood as maximized over constant offsets in time and phase (Δt_0 and $\Delta\phi_0$) between the two waveforms. The signal-to-noise ratio that would be obtained for a physical signal h_{e} and a model waveform h_{m} is then given by $\rho_{\mathrm{m}} = \langle h_{\mathrm{e}}|h_{\mathrm{m}}\rangle/\|h_{\mathrm{m}}\|$. It is related to the optimal signal-to-noise ratio ρ for a perfect model waveform by the *mismatch* $\mathcal{M}$ [118]:

$$\rho_{\rm m} = (1-\mathcal{M})\rho = (1-\mathcal{M})\langle h_{\rm e}|h_{\rm e}\rangle/\|h_{\rm e}\| \tag{11}$$

To leading order in $\|\delta h\|$, this definition of the mismatch implies [120,121]:

$$\mathcal{M} = \frac{\langle\delta h|\delta h\rangle - \langle\delta h_\parallel|\delta h_\parallel\rangle}{2\langle h_{\rm e}|h_{\rm e}\rangle} \leqslant \frac{\langle\delta h|\delta h\rangle}{2\langle h_{\rm e}|h_{\rm e}\rangle} \tag{12}$$

where $\delta h_\parallel = \langle\delta h|h_{\rm e}\rangle/\langle h_{\rm e}|h_{\rm e}\rangle$ is that part of the waveform error parallel to $h_{\rm e}$.

Based on these definitions, accuracy requirements are obtained as follows. Two waveforms differing by δh will be indistinguishable for a detector if $\langle\delta h|\delta h\rangle < 1$ [120,122], such that acceptable waveform models to be used in parameter estimation must lie within a sphere of unit radius of the exact waveform. For the purpose of event detection, a mismatch $\mathcal{M} = 3\%\ldots3.5\%$ is typically deemed acceptable. For detection efficiency, there arises, however, a complication due to the discrete nature of the template bank. In consequence, Lindblom et al. [120] recommend a maximum mismatch $\mathcal{M}_{\rm max} = 0.005$. In terms of the right-hand side of Eq. (12), dubbed *inaccuracy function* in Ref. [122], we summarize the accuracy requirements as

$$\frac{\|\delta h\|}{\|h\|} < \begin{cases} 1/\rho & \text{for parameter estimation} \\ \sqrt{2\mathcal{M}_{\rm max}} & \text{for detection} \end{cases} \tag{13}$$

Accuracy measurements employing the mismatch or $\|\delta h\|$ have been used to study numerical, semi-analytic and hybrid waveforms. According to the Samurai project [123], relative mismatches of the $l = m = 2$ mode between a variety of purely numerical waveforms for binaries with total mass $M \geqslant 60\ M_\odot$ are better than 10^{-3}. Hannam et al. [124] found errors in the construction of hybrid waveforms to be dominated by PN contributions. Numerical waveforms should be long enough to enable matching at lower frequencies, where PN approximations are more accurate: ~ 3 orbits before merger for the equal-mass, nonspinning case, and ~ 10 orbits for binaries with spins $\chi = 0.5$. MacDonald et al. [121] report significantly more demanding requirements of ~ 30 orbits for nonspinning, equal-mass binaries. Similarly, Boyle [125] concludes that longer NR waveforms or more accurate PN predictions will be required. The discrepancy largely arises from the use of more stringent accuracy thresholds: $\mathcal{M}_{\rm max} = 0.005$ in [121] (instead of $\mathcal{M}_{\rm max} = 0.03$ in [124]) for detection, and $\rho = 40$ for parameter estimation.

A comparison of phenomenological and EOB template banks based on the inaccuracy function has been performed by Damour et al. [122]. For advanced ground-based detectors, they conclude that current phenomenological models deviate from the EOB (considered as a target model) beyond acceptable thresholds over a wide range of the parameter space, for both, detection and parameter estimation.

4. Numerical relativity and astrophysics

Astrophysical observations of X-ray binaries or quasars, as mentioned in Section 1, have a good deal to tell us about BHs. In recent years, numerical relativity simulations of BHs have also deepened our insight into a variety of astrophysical systems.

4.1. Expected BH populations

We have already mentioned the two main classes of BHs identified by astrophysical observations. (i) Solar-mass BHs with $M \sim 5$–$20\ M_\odot$ are usually found in X-ray binaries [126] and are formed as the end-product of the evolution of massive stars. (ii) SMBHs with $M \sim 10^6$–$10^{9.5}\ M_\odot$ are believed to reside in most Active Galactic Nuclei (AGN) [9]. The assembly of these SMBHs is likely to result from a combination of BH mergers and accretion of surrounding matter over cosmological timescales. Evidence for a third class of BHs with $M \sim 10^2$–$10^5\ M_\odot$ (IMBHs) is tentative at present [127–129].

GW frequencies are inversely proportional to the system's total mass, and therefore BH masses play a crucial role in binary BH detectability. As discussed in the previous section, the expected GW pattern from BH binaries depends on the masses and spins of the binary members. We shall further see below that the gravitational recoil imparted upon the remnants of coalescing binaries strongly depends on spins and mass ratio.

Current spin estimates for accreting, stellar-mass BHs are usually obtained by modeling the shape of their X-ray spectrum or by analyzing the skew in Fe Kα emission lines. The resulting estimates are all, to some extent, model-dependent, but frequently yield moderate values $\chi \approx 0.1\ldots0.8$ and, for some cases, values close to the Kerr limit $\chi = 1$; see e.g. [24,130] and references therein. For SMBHs, spin estimates relying on the shape of the Fe Kα line yield values ranging from moderate $\chi \sim 0.6\ldots0.8$ (e.g. [131–133]) to near-critical spins (e.g. [134–137]). SMBHs are expected to grow by a combination of mergers and accretion. Their spin depends sensitively on the details of these processes and of their growth [138–140]. In any case, BH spins encode the history of their formation, and it would be extremely useful to have detailed knowledge of the BH spin distribution function. Ultimately, such a detailed census of BH parameters is one of the key targets of future GW observations [141,142]. For the purpose of numerical modeling of BHs, present measurements indicate that all spin magnitudes ($0 \leqslant \chi \leqslant 1$) should be covered.

We have already noted that stellar-mass BHs typically have masses in the range $[5, 20]\ M_\odot$. Unfortunately, there are no confirmed observations of stellar-mass *binary* BH candidates, so estimates of mass ratios must rely on theoretical models. For

stellar-mass binaries, population synthesis codes suggest that q should always be quite close to unity [143]. Measurements of SMBH masses are obtained by observations of stellar motion near galactic centers, as mentioned in Section 1, as well as motion of gas discs [144], applications of the virial theorem to the velocity dispersion of stars [145] and reverberation mappings applied to more distant AGNs [146]. An exhaustive list of galaxies with SMBH mass measurements in the range $M \sim 10^5$–$10^9\ M_\odot$ is presented by Graham et al. [147,148]. The general consensus is that mass ratios $q \lesssim 1/10$ (and down to $q \approx 10^{-4}$) should be common [19,149,150].

As in the case of BH spins, the observations imply that numerical relativity needs to cover a wide range in q.

From this discussion, it is clear that a detailed knowledge of the spin evolution as well as the generation of gravitational recoil in BH binary mergers is important for understanding the cosmological evolution of SMBHs over cosmological times. We will discuss these effects in turn.

4.2. Black-hole spins resulting from mergers

Numerical merger simulations showed that the merger of comparable-mass, nonspinning BHs leads to a final Kerr BH with spin parameter $a/M = 0.69$. The simulations were followed by the development of several models to predict the spin of merger remnants as a function of the binary parameters for generic mass ratios and spins.

The first studies focussed on performing numerical evolutions of the last few orbits of BH binaries, and used the results to calibrate formulae that map the initial binary parameters to values for the spin of the merged hole [73,82,151–154]. It became clear, however, that the binary inspiral up to the last orbits has the potential to significantly affect the spin distribution (e.g. [155]) and therefore should be included, for example via PN modeling, in the derivation of maps from initial parameters to the merger remnant properties [156–160]. A comprehensive review of all spin formulae is beyond the scope of this article, but we refer the reader to the review in [161] and the discussion in Section V of [160]. If we assume an ensemble of BH binaries with initially randomly oriented spins, the final spin distribution is peaked around $\chi_f \approx 0.7$ [140,156,159]. Campanelli et al. [151,162] reported spin flips by 34–103° with respect to the initial spin direction of the larger hole; spin flips of this magnitude could provide an explanation for X-shaped radio sources [163]. Kesden et al. [160] demonstrated that spin precession over the course of a long inspiral of thousands of orbits tends to align (anti-align) the binary BH spins with each other if the spin of the more massive BH is initially partially aligned (anti-aligned) with the orbital angular momentum, thus increasing (decreasing) the average final spin.

4.3. Gravitational recoil

One of the most spectacular results obtained from numerical BH binary simulations is the quantitative prediction of the magnitude of *gravitational recoils* (or *kicks*). In the 1960s it was realized that the emission of linear momentum via GWs must impart a kick on the source due to momentum conservation [164,165]. However, the astrophysical relevance of the gravitational recoil following BH binary mergers remained an open question until the recent numerical relativity breakthroughs.

For the case of an equal-mass, nonspinning BH binary, the net linear momentum emitted in GWs vanishes due to symmetry. Nonzero recoils are therefore only generated in systems where this symmetry is broken through (i) a mass ratio $q < 1$ (equivalently, a symmetric mass ratio parameter $\eta \equiv q/(1+q)^2 < 1/4$) or (ii) nonvanishing spins.

For zero spins, early numerical studies in the range $q = [1, 1/4]$ found that the kick velocity is well approximated by [166–168]

$$v_{\rm kick} = 1.2 \times 10^4 \eta^2 \sqrt{1-4\eta}(1 - 0.93\eta)\ \text{km/s} \tag{14}$$

The maximal recoil obtained from Eq. (14) is $v_{\rm max} = 175.2 \pm 11$ km/s for $q = 0.36 \pm 0.03$.

Spinning binaries are characterized by seven free parameters (the mass ratio plus three components for each BH spin), and numerical studies inevitably focussed on subsets of the parameter space. It soon became clear that the spin interaction dominates over mass ratio effects. The first studies for equal-mass binaries with spins parallel to the orbital angular momentum revealed kicks of several hundreds km/s, with an extrapolated maximum of ~ 500 km/s for extremal spin magnitudes [169,170]. Shortly thereafter, the discovery of the so-called *superkicks* marked one of the most surprising outcomes of numerical relativity: binaries for which the spins are perpendicular to the orbital angular momentum and anti-aligned with each other can generate kicks of *thousands* of km/s, with an extrapolated maximum $v_{\rm max} \sim 4000$ km/s for near-extremal spin magnitudes [162,171,172].

Many galaxies harbor SMBHs at their centers, and galaxy mergers should generally lead to the merger of their central BHs [173]. Typical escape velocities range from ~ 10 km/s for dwarf galaxies up to ~ 1000 km/s for giant elliptic galaxies [174]. Large kicks would displace or eject the merged hole from its host, with possibly observable consequences. BH ejection represents a potential obstacle for BH growth via merger, and thus puts constraints on merger-history models, which must be able to explain the assembly of SMBHs by redshifts $z \gtrsim 6$ [175–177]. Observed redshifts of broad-line relative to narrow-line regions in quasar spectra may be interpreted as a smoking gun of BH ejection due to gravitational recoil [178–180].

The interest in astrophysical consequences of large recoils led to numerical studies of the BH parameter space [74,181–189]. Phenomenological kick formulas inspired by PN studies [87] and similar to Eq. (14) were proposed to map the input

parameters of a given binary configuration to the final kick velocity. Available numerical results are well described by Eq. (2) of Ref. [162] (see also [158,190]).

The apparent incompatibility between large recoils and the existence of BHs at galactic centers can be resolved by mechanisms that would *align* the individual BH spins with the orbital angular momentum of the binary. One such mechanism are gas torques in the so-called "wet" (gas-rich) mergers, that would produce partial alignment "early on" in the inspiral phase [191]. If partial alignment in gas-rich mergers is the norm, as suggested also by the spin measurements discussed above, PN spin effects will lead to *further* alignment of the spins with the orbital angular momentum, significantly reducing the typical values of recoil velocities [155,192].

4.4. Merger simulations with matter and the Blandford–Znajek effect

Many numerical relativity groups are presently working on binary BH simulations in the presence of matter. Most of this work is trying to understand the signature of electromagnetic counterparts to binary BH mergers: for example, such a signature could be produced by merger events [193] or recoiling BHs [194] "shocking" the surrounding accretion disks. The Georgia Tech group presented the first simulations in full GR of equal-mass, spinning BHs merging in a gas cloud. They found that shocks, accretion and relativistic beaming can produce electromagnetic signatures correlated with GWs, especially when spins are aligned with the orbital axis [195–197]. The Urbana group simulated equal-mass, nonspinning BH binaries embedded in gas clouds under different assumptions for the motion of the binary with respect to the gas. They found evidence that the accretion rate and luminosity due to bremsstrahlung and synchrotron emission would be enhanced with respect to a single BH of the same mass as the binary [198]. Recent work suggests that the circumbinary disk surrounding BH binaries should not produce detectable electromagnetic counterparts [197,199]. However, the *magnetic field* produced by the circumbinary disk may extract energy from the orbiting BHs, which ultimately merge within the standard Blandford–Znajek scenario, generating electromagnetic emission along dual or single jets that could be observable to large distance [200–203].

5. Conclusions

We conclude this review with a brief summary of the most urgent problems to be tackled by numerical relativity in the two main areas in the near future.

Gravitational wave physics In order to meet tight accuracy requirements in GW template generation, especially for parameter estimation, we either need longer numerical waveforms or a denser spacing of templates in the parameter space. Both approaches will require computational resources that grow nonlinearly as a function of the accuracy, either because of the slow nature of the inspiral at larger BH separations (see Section 2 in [121] for a quantitative discussion) or because of the dimensionality of the parameter space. A second major task is the extension of existing template models to generic binaries with precessing spins and/or smaller mass ratios, bridging the gap to perturbative modeling of extreme mass ratio binaries.

Astrophysics While existing formulae for the kick and final spin resulting from the coalescence of BHs have been helpful for astrophysical studies, the calibration of generic models as proposed by Boyle et al. [204,205] requires a more comprehensive exploration of the parameter space. The relatively young field of numerical relativity simulations of BHs surrounded by accretion disks will likely improve our insight into expected optical counterparts to BH binary mergers, and thus provide a vital tool for the area of *multi-messenger astrophysics*.

Acknowledgements

U.S. acknowledges support from the Ramón y Cajal Programme of the Ministry of Education and Science of Spain, the FP7-PEOPLE-2011-CIG Grant *CBHEO 293412*, NSF grants PHY-0601459, PHY-0652995 and the Sherman Fairchild Foundation to Caltech. E.B.'s research is supported by the NSF grant PHY-0900735 and by the NSF CAREER grant PHY-1055103. This work was supported by the *DyBHo-256667* ERC Starting Grant, by the FP7-PEOPLE-2011-IRSES Grant *NRHEP 295189* and by FCT-Portugal through projects PTDC/FIS/098025/2008, PTDC/FIS/098032/2008, CTE-AST/098034/2008 and CERN/FP/116341/2010. We acknowledge support by and allocations through the TeraGrid Advanced Support Program at the San Diego Supercomputing Center and the National Institute for Computational Sciences under grant PHY-090003, the Centro de Supercomputación de Galicia (CESGA) under project numbers ICTS-CESGA-175 and ICTS-CESGA-200, the Barcelona Supercomputing Center (BSC) under project AECT-2011-2-0006 and the DEISA Extreme Computing Initiative (DECI-6).

References

[1] R. Giacconi, et al., Phys. Rev. Lett. 9 (1963) 439–443.
[2] I.S. Shklovsky, Astrophys. J. 148 (1967) L1–L4.
[3] J. van Paradijs, in: American Astronomical Society Meeting Abstracts, in: Bulletin of the American Astronomical Society, vol. 30, 1998, p. 1291.
[4] T.A. Matthews, A.R. Sandage, Astrophys. J. 138 (1963) 30.
[5] M. Schmidt, Nature 197 (1963) 1040.

[6] E.E. Salpeter, Astrophys. J. 140 (1964) 796–800.
[7] Y.B. Zel'dovich, I.D. Novikov, Dokl. Akad. Nauk SSSR 155 (1964) 57.
[8] M.J. Rees, Phys. Scr. 17 (1978) 193–200.
[9] F. Melia, arXiv:0705.1537 [astro-ph].
[10] LIGO website, http://www.ligo.org.
[11] VIRGO website, https://wwwcascina.virgo.infn.it/.
[12] GEO600 website, http://www.geo600.org/.
[13] ESA-LISA website, http://www.esa.int/esaSC/120376_index_0_m.html.
[14] L.S. Finn, Phys. Rev. D 46 (1992) 5236–5249.
[15] J. Abadie, et al., Class. Quantum Grav. 27 (2010) 173001.
[16] T. Bulik, K. Belczynski, A. Prestwich, Astrophys. J. 730 (2011) 140.
[17] M. Volonteri, F. Haardt, P. Madau, Astrophys. J. 582 (2003) 559–573.
[18] M.C. Begelman, M. Volonteri, M.J. Rees, Mon. Not. R. Astron. Soc. 370 (2006) 289–298.
[19] A. Sesana, M. Volonteri, F. Haardt, Mon. Not. R. Astron. Soc. 377 (2007) 1711–1716.
[20] K.G. Arun, et al., arXiv:0811.1011 [gr-qc].
[21] L. Blanchet, Living Rev. Relativ. 9 (2006), 4, http://www.livingreviews.org/lrr-2006-4.
[22] S.A. Teukolsky, Astrophys. J. 185 (1973) 635–648.
[23] E.W. Leaver, Phys. Rev. D 34 (1986) 384–408.
[24] E. Berti, V. Cardoso, A.O. Starinets, Class. Quantum Grav. 26 (2009) 163001.
[25] F. Pretorius, Phys. Rev. Lett. 95 (2005) 121101.
[26] M. Campanelli, et al., Phys. Rev. Lett. 96 (2006) 111101.
[27] J.G. Baker, et al., Phys. Rev. Lett. 96 (2006) 111102.
[28] R. Arnowitt, S. Deser, C.W. Misner, in: L. Witten (Ed.), Gravitation: An Introduction to Current Research, John Wiley, New York, 1962, pp. 227–265.
[29] J.W. York Jr., in: L. Smarr (Ed.), Sources of Gravitational Radiation, Cambridge University Press, Cambridge, 1979, pp. 83–126.
[30] M. Alcubierre, Introduction to 3+1 Numerical Relativity, Oxford University Press, Oxford, 2008.
[31] M. Shibata, T. Nakamura, Phys. Rev. D 52 (1995) 5428–5444.
[32] T.W. Baumgarte, S.L. Shapiro, Phys. Rev. D 59 (1998) 024007.
[33] M. Alcubierre, et al., Phys. Rev. D 67 (2003) 084023.
[34] J.R. van Meter, et al., Phys. Rev. D 73 (2006) 124011.
[35] D. Müller, J. Grigsby, B. Brügmann, Phys. Rev. D 82 (2010) 064004.
[36] D. Alic, et al., Class. Quantum Grav. 27 (2010) 245023.
[37] Y. Fourés-Bruhat, Acta Math. 88 (1952) 141–225.
[38] Y. Bruhat, in: L. Witten (Ed.), Gravitation: An Introduction to Current Research, John Wiley, New York, 1962, pp. 130–168.
[39] A.E. Fischer, J.E. Marsden, Commun. Math. Phys. 28 (1972) 1–38.
[40] H. Friedrich, Commun. Math. Phys. 100 (1985) 525.
[41] D. Garfinkle, Phys. Rev. D 65 (2002) 044029.
[42] C. Gundlach, et al., Class. Quantum Grav. 22 (2005) 3767–3773.
[43] M.A. Scheel, et al., Phys. Rev. D 74 (2006) 104006.
[44] M. Boyle, et al., Phys. Rev. D 76 (2007) 124038.
[45] L. Lindblom, et al., Class. Quantum Grav. 23 (2006) S447–S462.
[46] M. Boyle, et al., Phys. Rev. D 78 (2008) 104020.
[47] T. Chu, et al., Phys. Rev. D 80 (2009) 124051.
[48] G.B. Cook, Living Rev. Relativ. 3 (2000), 5, http://www.livingreviews.org/lrr-2000-5.
[49] A. Lichnerowicz, J. Math. Pures Appl. 23 (1944) 37–63.
[50] C.W. Misner, Phys. Rev. 118 (1960) 1110.
[51] D.R. Brill, R.W. Lindquist, Phys. Rev. 131 (1963) 471–476.
[52] J.M. Bowen, J.W. York Jr., Phys. Rev. D 21 (1980) 2047–2056.
[53] S. Brandt, B. Brügmann, Phys. Rev. Lett. 78 (1997) 3606–3609.
[54] G.B. Cook, H. Pfeiffer, Phys. Rev. D 70 (2004) 104016.
[55] S. Dain, J.L. Jaramillo, B. Krishnan, Phys. Rev. D 71 (2004) 064003.
[56] A. Ashtekar, B. Krishnan, Living Rev. Relativ. 7 (2004), 10, http://www.livingreviews.org/lrr-2004-10.
[57] A. Buonanno, G.B. Cook, F. Pretorius, Phys. Rev. D 75 (2007) 124018.
[58] E. Gourgoulhon, arXiv:gr-qc/0703035.
[59] T.W. Baumgarte, et al., Phys. Rev. D 54 (1996) 4849.
[60] P. Anninos, et al., Phys. Rev. D 58 (1998) 024003.
[61] J. Thornburg, Class. Quantum Grav. 21 (2004) 743–766.
[62] B. Krishnan, Class. Quantum Grav. 25 (2008) 114005.
[63] E.T. Newman, R. Penrose, J. Math. Phys. 3 (1962) 566–578.
[64] W. Kinnersley, J. Math. Phys. 10 (1969) 1195–1203.
[65] B. Brügmann, et al., Phys. Rev. D 77 (2008) 024027.
[66] T. Regge, J.A. Wheeler, Phys. Rev. 108 (1957) 1063–1069.
[67] F.J. Zerilli, J. Math. Phys. 11 (1970) 2203–2208.
[68] F.J. Zerilli, Phys. Rev. Lett. 24 (1970) 737–738.
[69] C. Reisswig, et al., Phys. Rev. D 83 (2011) 064008.
[70] A. Buonanno, Y. Chen, M. Vallisneri, Phys. Rev. D 67 (2003) 024016;
A. Buonanno, Y. Chen, M. Vallisneri, Phys. Rev. D 74 (2006) 029903 (Erratum).
[71] C.O. Lousto, et al., Phys. Rev. D 82 (2010) 104057.
[72] C.O. Lousto, Y. Zlochower, Phys. Rev. Lett. 106 (2011) 041101.
[73] P. Marronetti, et al., Phys. Rev. D 77 (2008) 064010.
[74] S. Dain, C.O. Lousto, Y. Zlochower, Phys. Rev. D 78 (2008) 024039.
[75] G. Lovelace, et al., Phys. Rev. D 78 (2008) 084017.
[76] M.D. Hannam, et al., Class. Quantum Grav. 24 (2007) S15–S24.
[77] Y.T. Liu, Z.B. Etienne, S.L. Shapiro, Phys. Rev. D 80 (2009) 121503.
[78] G. Lovelace, M.A. Scheel, B. Szilagyi, Phys. Rev. D 83 (2011) 024010.

[79] P.C. Peters, J. Mathews, Phys. Rev. 131 (1963) 435–439.
[80] U. Sperhake, et al., Class. Quantum Grav. 28 (2011) 134004.
[81] M.A. Scheel, et al., Phys. Rev. D 79 (2009) 024003.
[82] E. Berti, et al., Phys. Rev. D 76 (2007) 064034.
[83] J.A. González, U. Sperhake, B. Brügmann, Phys. Rev. D 79 (2009) 124006.
[84] J.G. Baker, et al., Phys. Rev. D 78 (2008) 044046.
[85] M. Campanelli, C.O. Lousto, Y. Zlochower, Phys. Rev. D 74 (2006) 041501.
[86] I. Hinder, et al., Phys. Rev. D 82 (2010) 024033.
[87] L.E. Kidder, Phys. Rev. D 52 (1995) 821–847.
[88] R.P. Kerr, Phys. Rev. Lett. 11 (1963) 237–238.
[89] E.W. Leaver, Proc. R. Soc. Lond. A 402 (1985) 285–298.
[90] O. Dreyer, et al., Class. Quantum Grav. 21 (2004) 787–804.
[91] E. Berti, V. Cardoso, C.M. Will, Phys. Rev. D 73 (2006) 064030.
[92] E. Berti, et al., Phys. Rev. D 76 (2007) 104044.
[93] E. Berti, V. Cardoso, Phys. Rev. D 74 (2006) 104020.
[94] D. Keppel, P. Ajith, Phys. Rev. D 82 (2010) 122001.
[95] M. Salgado, et al., Phys. Rev. D 77 (2008) 104010.
[96] V. Paschalidis, et al., Class. Quantum Grav. 28 (2011) 085006.
[97] A. Buonanno, T. Damour, Phys. Rev. D 59 (1999) 084006.
[98] A. Buonanno, T. Damour, Phys. Rev. D 62 (2000) 064015.
[99] Y. Pan, et al., arXiv:1106.1021 [gr-qc].
[100] A. Buonanno, L.E. Kidder, L. Lehner, Phys. Rev. D 77 (2008) 026004.
[101] T. Damour, et al., Phys. Rev. D 77 (2008) 084017.
[102] T. Damour, et al., Phys. Rev. D 78 (2008) 044039.
[103] Y. Pan, et al., Phys. Rev. D 81 (2010) 084041.
[104] P. Ajith, et al., Class. Quantum Grav. 24 (2007) S689–S700.
[105] P. Ajith, et al., Phys. Rev. D 77 (2008) 104017.
[106] P. Ajith, Class. Quantum Grav. 25 (2008) 114033.
[107] P. Ajith, et al., arXiv:0909.2867 [gr-qc].
[108] L. Santamaria, et al., Phys. Rev. D 82 (2010) 064016.
[109] J. Abadie, et al., arXiv:1102.3781 [gr-qc].
[110] Ninja homepage, https://www.ninja-project.org/doku.php.
[111] B. Aylott, et al., Class. Quantum Grav. 26 (2009) 165008.
[112] B. Aylott, et al., Class. Quantum Grav. 26 (2009) 114008.
[113] NRAR homepage, https://www.ninja-project.org/doku.php?id=nrar:home.
[114] R.N. Lang, S.A. Hughes, N.J. Cornish, arXiv:1101.3591 [gr-qc].
[115] S.T. McWilliams, et al., arXiv:1104.5650 [gr-qc].
[116] M. Boyle, A.H. Mroué, Phys. Rev. D 80 (2009) 124045.
[117] L.S. Finn, D.F. Chernoff, Phys. Rev. D 47 (1993) 2198–2219.
[118] C. Cutler, E.E. Flanagan, Phys. Rev. D 49 (1994) 2658–2697.
[119] LIGO Document T0900288-v3, https://dcc.ligo.org/cgi-bin/DocDB/ShowDocument?docid=2974.
[120] L. Lindblom, J.G. Baker, B.J. Owen, Phys. Rev. D 82 (2010) 084020.
[121] I. MacDonald, S. Nissanke, H.P. Pfeiffer, Class. Quantum Grav. 28 (2011) 134002.
[122] T. Damour, M. Trias, A. Nagar, Phys. Rev. D 83 (2011) 024006.
[123] M. Hannam, et al., Phys. Rev. D 79 (2009) 084025.
[124] M. Hannam, et al., Phys. Rev. D 82 (2010) 124008.
[125] M. Boyle, arXiv:1103.5088 [gr-qc].
[126] R.A. Remillard, J.E. McClintock, Ann. Rev. Astron. Astrophys. 44 (2006) 49–92.
[127] M.C. Miller, E.J.M. Colbert, Int. J. Mod. Phys. D 13 (2004) 1–64.
[128] J.R. Hurley, Mon. Not. R. Astron. Soc. 379 (2007) 93–99.
[129] C.T. Berghea, et al., arXiv:0807.1547 [astro-ph].
[130] J.E. McClintock, et al., Class. Quantum Grav. 28 (2011) 114009.
[131] G. Miniutti, et al., arXiv:0905.2891 [astro-ph].
[132] S. Schmoll, et al., Astrophys. J. 703 (2009) 2171–2176.
[133] L.C. Gallo, et al., arXiv:1009.2987 [astro-ph].
[134] A.C. Fabian, et al., Mon. Not. R. Astron. Soc. 361 (2005) 795–802.
[135] L.W. Brenneman, C.S. Reynolds, Astrophys. J. 652 (2006) 1028–1043.
[136] A. Fabian, et al., arXiv:0905.4383 [astro-ph].
[137] L.W. Brenneman, et al., arXiv:1104.1172 [astro-ph].
[138] C.F. Gammie, S.L. Shapiro, J.C. McKinney, Astrophys. J. 602 (2004) 312–319.
[139] S.A. Hughes, R.D. Blandford, Astrophys. J. 585 (2003) L101–L104.
[140] E. Berti, M. Volonteri, Astrophys. J. 684 (2008) 822.
[141] I. Mandel, V. Kalogera, R. O'Shaughnessy, arXiv:1001.2583 [astro-ph].
[142] A. Sesana, et al., Phys. Rev. D 83 (2011) 044036.
[143] K. Belczynski, et al., Astrophys. J. 682 (2008) 474–486.
[144] J.R. Herrnstein, et al., Nature 400 (1999) 539–541.
[145] J. Kormendy, D. Richstone, Ann. Rev. Astron. Astrophys. 33 (1995) 581–624.
[146] K. Gebhardt, et al., Astrophys. J. 543 (2000) L5.
[147] A.W. Graham, Publ. Astron. Soc. Aust. 25 (2008) 167–175.
[148] A.W. Graham, et al., arXiv:1007.3834 [astro-ph].
[149] S.M. Koushiappas, A.R. Zentner, Astrophys. J. 639 (2006) 7.
[150] L.A. Gergely, B. Mikoczi, Phys. Rev. D 79 (2009) 064023.
[151] M. Campanelli, et al., Phys. Rev. D 75 (2007) 064030.
[152] L. Rezzolla, et al., Astrophys. J. 679 (2008) 1422.

[153] L. Rezzolla, et al., Astrophys. J. 674 (2008) L29–L32.
[154] L. Rezzolla, et al., Phys. Rev. D 78 (2008) 044002.
[155] J.D. Schnittman, Phys. Rev. D 70 (2004) 124020.
[156] W. Tichy, P. Marronetti, Phys. Rev. D 78 (2008) 081501.
[157] E. Barausse, L. Rezzolla, Astrophys. J. 704 (2009) L40–L44.
[158] C.O. Lousto, M. Campanelli, Y. Zlochower, Class. Quantum Grav. 27 (2010) 114006.
[159] C.O. Lousto, et al., Phys. Rev. D 81 (2010) 084023.
[160] M. Kesden, U. Sperhake, E. Berti, Phys. Rev. D 81 (2010) 084054.
[161] L. Rezzolla, Class. Quantum Grav. 26 (2009) 094023.
[162] M. Campanelli, et al., Astrophys. J. 659 (2007) L5–L8.
[163] D. Merritt, R.D. Ekers, Science 297 (2002) 1310–1313.
[164] W.B. Bonnor, M.A. Rotenberg, Proc. R. Soc. Lond. A 265 (1961) 109–116.
[165] A. Peres, Phys. Rev. 128 (1962) 2471–2475.
[166] F. Herrmann, et al., Class. Quantum Grav. 24 (2007) S33–S42.
[167] J.G. Baker, et al., Astrophys. J. 653 (2006) L93–L96.
[168] J.A. González, et al., Phys. Rev. Lett. 98 (2007) 091101.
[169] F. Herrmann, et al., Astrophys. J. 661 (2007) 430.
[170] M. Koppitz, et al., Phys. Rev. Lett. 99 (2007) 041102.
[171] J.A. González, et al., Phys. Rev. Lett. 98 (2007) 231101.
[172] M. Campanelli, et al., Phys. Rev. Lett. 98 (2007) 231102.
[173] M.C. Begelman, R.D. Blandford, M.J. Rees, Nature 287 (1980) 307–309.
[174] D. Merritt, et al., Astrophys. J. 607 (2004) L9–L12.
[175] Z. Haiman, Astrophys. J. 613 (2004) 36–40.
[176] Y. Li, et al., Astrophys. J. 665 (2007) 187–208.
[177] M. Volonteri, K. Gültekin, M. Dotti, Mon. Not. R. Astron. Soc. 404 (2010) 2143–2150.
[178] S. Komossa, H. Zhou, H. Lu, Astrophys. J. 678 (2008) L81.
[179] F. Civano, et al., Astrophys. J. 717 (2010) 209–222.
[180] A. Robinson, et al., Astrophys. J. 717 (2010) L122–L126.
[181] W. Tichy, P. Marronetti, Phys. Rev. D 76 (2007) 061502(R).
[182] J.G. Baker, et al., Astrophys. J. 668 (2008) 1140–1144.
[183] B. Brügmann, et al., Phys. Rev. D 77 (2008) 124047.
[184] C.O. Lousto, Y. Zlochower, Phys. Rev. D 77 (2008) 044028.
[185] D. Pollney, et al., Phys. Rev. D 76 (2007) 124002.
[186] J.G. Baker, et al., Astrophys. J. 682 (2008) L29.
[187] C.O. Lousto, Y. Zlochower, Phys. Rev. D 79 (2009) 064018.
[188] C.O. Lousto, Y. Zlochower, Phys. Rev. D 83 (2010) 024003.
[189] Y. Zlochower, M. Campanelli, C.O. Lousto, arXiv:1011.2210 [gr-qc].
[190] J.R. van Meter, et al., arXiv:1003.3865 [astro-ph].
[191] T. Bogdanović, C.S. Reynolds, M.C. Miller, Astrophys. J. 661 (2007) L147–L150.
[192] M. Kesden, U. Sperhake, E. Berti, Astrophys. J. 715 (2010) 1006–1011.
[193] M. Megevand, et al., Phys. Rev. D 80 (2009) 024012.
[194] M. Anderson, et al., Phys. Rev. D 81 (2010) 044004.
[195] T. Bode, et al., Astrophys. J. 715 (2010) 1117–1131.
[196] T. Bogdanovic, et al., Class. Quantum Grav. 28 (2011) 094020.
[197] T. Bode, et al., arXiv:1101.4684 [astro-ph].
[198] B.D. Farris, Y.T. Liu, S.L. Shapiro, Phys. Rev. D 81 (2010) 084008.
[199] P. Mösta, et al., Phys. Rev. D 81 (2010) 064017.
[200] C. Palenzuela, et al., Phys. Rev. Lett. 103 (2009) 081101.
[201] C. Palenzuela, L. Lehner, S. Yoshida, Phys. Rev. D 81 (2010) 084007.
[202] C. Palenzuela, L. Lehner, S.L. Liebling, Science 329 (2010) 927.
[203] C. Palenzuela, et al., Phys. Rev. D 82 (2010) 044045.
[204] L. Boyle, M. Kesden, S. Nissanke, Phys. Rev. Lett. 100 (2008) 151101.
[205] L. Boyle, M. Kesden, Phys. Rev. D 78 (2008) 024017.